UW CPTC Report 10-7:
Peak neoclassical toroidal viscosity at low toroidal rotation in the DIII-D tokamak

A. J. Cole[1], J. D. Callen[1], W. M. Solomon[2], A. M. Garofalo[3],
C. C. Hegna[1], M. J. Lanctot[4], H. Reimerdes[4], and and the DIII-D Team
[1] *University of Wisconsin, 1500 Engineering Dr., Madison, Wisconsin 53706-1609, USA*
[2] *Princeton Plasma Physics Laboratory, P.O. Box 451, Princeton, New Jersey 08543-0451, USA*
[3] *General Atomics, P.O. Box 85608, San Diego, California 92186-5608, USA*
[4] *Columbia University, 2960 Broadway, New York, New York 10027-1754, USA**

(Dated: April 28, 2011)

Abstract

Observation of a theoretically-predicted peak in the neoclassical toroidal viscous [NTV] force as a function of toroidal plasma rotation rate Ω is reported. The NTV was generated by applying $n = 3$ magnetic fields from internal (I-)coils to low Ω plasmas produced with nearly balanced neutral beam injection. Locally, the peak corresponds to a toroidal rotation rate Ω_0 where the radial electric field E_r is near zero as determined by radial ion force balance.

PACS numbers: 52.25.Xz, 51.20.+d, 52.25.Fi, 52.55.Fa, and 52.55.Hc

*Electronic address: acole@cae.wisc.edu

I. INTRODUCTION

Understanding the influence of non-axisymmetric magnetic fields on toroidal plasma rotation remains a fundamental challenge of fusion plasma science. In this paper we investigate the toroidal rotation dependence of neoclassical toroidal viscosity (NTV) driven by non-axisymmetric magnetic perturbations (i.e., those which have some toroidal angular dependence). Non-axisymmetric magnetic fields are always present, stemming from either machine errors in coil alignment, current leads, etc., of the order of $\delta B/B_0 \sim 10^{-4}$, or from magnetohydrodynamic (MHD) mode activity, with $\delta B/B_0 \sim 10^{-3}$. Here $B_0 \sim 1-2$ Tesla is the typical equilibrium magnetic field strength for present tokamaks such as DIII-D [1].

Non-axisymmetric magnetic perturbations can affect plasma rotation in toroidally confined plasmas either by inducing resonant localized electromagnetic torques on rational surfaces, or through their modification of $|\vec{B}|$. In this latter case, variations along a field line induce non-ambipolar radial particle transport and produce a global NTV force [2] which tries to rotate the plasma at a diamagnetic-like rotation rate. Rotation in toroidal plasmas [3] benefits confinement and stability by shielding resonant magnetic perturbations, stabilizing resistive wall modes, and reducing transport. For these reasons, NTV has generated considerable experimental interest [4–8], as it promises to provide an external input for toroidal rotation without inducing locked modes. Such capability would be a great benefit to ITER, since its present benchmark scenario [9] relies on an ohmic start up with an anticipated low toroidal rotation rate (~ 0.5 kHz), compared to present tokamaks.

II. THEORETICAL MOTIVATION

Breaking toroidal symmetry introduces bounce-averaged mirror and curvature forces with toroidal components that when crossed with the equilibrium magnetic field generate non-ambipolar radial particle and heat fluxes. In a fluid moment approach [10] toroidal forces arising from symmetry breaking appear as a modification to the parallel stress tensor, generating a *toroidal* viscous force which is absent in the limit of perfect axisymmetry. When the non-axisymmetric magnetic field amplitude is much less than the poloidal mirror trapping, i.e., $\delta B/B_0 \ll \epsilon = r/R_0$ with r (R_0) the minor (major) axis of the tokamak, poloidal and *toroidal* plasma flows on magnetic flux surfaces can be determined succes-

sively [11, 12]. First, on the ion-ion collision timescale $1/\nu_i$ ($\sim$ ms), the parallel force balance equation describes the damping of poloidal flow to a diamagnetic-like rate given by $\left\langle q\vec{V}_i \cdot \vec{\nabla}\theta \right\rangle \simeq (c_p/Z_i e) dT_i/d\chi$. ($c_p$ is often labeled k_i [13].) Here $\vec{V}_i$ is the ion fluid velocity, T_i is the ion temperature, $Z_i e$ is the dominant ion species charge, χ is the poloidal magnetic flux function, $q = \vec{B} \cdot \vec{\nabla}\zeta / \vec{B} \cdot \vec{\nabla}\theta = d\Psi/d\chi$ is the toroidal "safety factor," θ (ζ) is a poloidal (toroidal) angle, c_p is a number of order unity, and $\langle \dots \rangle$ denotes a flux surface average. Second, on a longer transport timescale roughly of order $[(\mathrm{v}_{ti}/R_0)\,(\delta B_n/B_0)^2]^{-1}$, with $v_{ti} \equiv \sqrt{2T_i/m_i}$ the ion thermal speed, the non-axisymmetric magnetic fields damp the *toroidal* component of plasma flow to a rotation rate $\Omega_*(\nu_i, E_r) = [(c_t + c_p)/(Z_i e)] dT_i/d\chi$, where c_t is a number of order unity. In this two-stage successive determination of the plasma flows, the rate of change in the toroidal rotation from NTV alone is of the form [11, 14, 15]

$$\left.\frac{\partial \Omega}{\partial t}\right|_{NTV} = -\mu_{\|}(\nu_i, E_r) \left\langle \frac{\delta B_n^2}{B_0^2} \right\rangle \left[\Omega - \Omega_*(\nu_i, E_r) \right] \quad . \tag{1}$$

Here $\langle \delta B_n^2 / B_0^2 \rangle$ is the relative amplitude of the non-axisymmetric fields, $\Omega \equiv \left\langle R^2 \vec{V} \cdot \vec{\nabla}\zeta \right\rangle / \langle R^2 \rangle$, and $\mu_{\|}(\nu_i, E_r)$ is the NTV damping rate.

Experiments on DIII-D [7], JET [4], NSTX [5, 8], and MAST [16] have all observed toroidal flow damping with the application of external non-axisymmetric fields in general agreement with the form given in Eq. (1). With the recent introduction of both co- and counter-I_p (plasma current) neutral beam injection, the DIII-D tokamak is now able to access low toroidal rotation states and observe both toroidal flow damping and spin-up [6, 17], to an offset value in qualitative agreement with Ω_* defined in Eq. (5) below.

In this paper, we expand on previous work by performing a rotation scan of the NTV torque applied by external non-resonant $n = 3$ fields from the I-coils [18] on the DIII-D tokamak. Varying the toroidal precessional drift relative to other characteristic frequencies of interest causes a change in the level of NTV damping [2, 19, 20]. As will be shown below, scanning toroidal rotation is equivalent to varying the radial electric field, and thus will induce a transition between asymptotic NTV collisionality regimes of interest to tokamaks.

Time scales longer than compressional Alfvén wave times ($\sim \mu$s) require radial force balance, which yields [11, 12]

$$\omega_E = \frac{\left\langle q R^2 \vec{V}_i \cdot \vec{\nabla}\theta \right\rangle}{\langle R^2 \rangle} - \frac{1}{Z_i e n_i} \left(\frac{dp_i}{d\chi} \right) - \Omega \equiv \Omega_0 - \Omega \quad , \tag{2}$$

where $\omega_E \equiv d\phi/d\chi \simeq E_r/(RB_\theta)$ is the toroidal $\vec{E}\times\vec{B}$ precessional drift frequency. If the plasma profiles are assumed to remain fixed, then Eq. (2) indicates that scanning Ω will cause a concomitant change in E_r. This will in turn vary the critical collisionality ratio ν_i/ω_E, and cause transitions between the relevant NTV regimes.

III. THEORETICAL MODEL

For DIII-D high confinement (H)-mode plasmas, the ion collision rate is much smaller than both the toroidal transit frequency and the bounce frequency of particles trapped in the $1/R$ variation of the magnetic field. Under these conditions, the trapped particle orbits are influenced by the small non-axisymmetric fields and their resulting magnetic drifts determine the level of neoclassical toroidal viscosity in the plasma (see the regimes labeled "3D" in Fig. 1). In each of the relevant regimes, different effects limit the radial excursions of the trapped ion banana orbit centers and their effects on the perturbed parallel ion viscosity. The first such non-axisymmetric regime encountered is the $1/\nu$ regime where collisions limit the trapped ion radial drifts [2]. As the effective ion collisionality $\nu_{\rm eff} = \nu_i/\left(|n|\epsilon\right)$ continues to decrease, two effects can limit the radial transport/toroidal torque on the plasma. The first is a collisional boundary layer at the trapped-passing boundary which occurs when $\nu_{\rm eff} \ll \dot{\zeta}_0$ [19]. Here $\dot{\zeta}_0 = \omega_E + \omega_{\vec{\nabla}B} \sim \omega_E$ is the trapped particle toroidal precession frequency, composed of both the $\vec{E}\times\vec{B}$ drift defined immediately after Eq. (2), and the magnetic toroidal precessional drift $\omega_{\vec{\nabla}B}$ defined in Eq. (A38). The second effect to limit the toroidal torque on the plasma occurs when $\nu_{\rm eff} \ll \dot{\zeta}_0$ *and* the radial electric field becomes small enough that ω_E is of the order of $\omega_{\vec{\nabla}B}$ (see Eq. (A38)). Under these conditions, resonances in the toroidal precessional drift can occur, i.e., $\dot{\zeta}_0 = 0$ which dominate the neoclassical toroidal viscosity. This regime is known as the *superbanana plateau* [sbp] [20], since trapped particles with zero precessional drift have formally unbounded radial excursions from a flux surface, hence "super-bananas," and the resonance is resolved via collisions leading to plateau-like transport. All three of these low collisionality NTV regimes diverge outside of the their region of applicability in $\nu_i - \omega_E$ parameter space. While there is no unique method to connect them, a simple way to construct a NTV torque which smoothly transitions between all the asymptotic regimes is by inverse addition. This method generates a Padé approximate

NTV torque valid over all three collisionality regimes:

$$\frac{\partial \Omega}{\partial t} = -\mu_{\|\mathrm{P}}(\Omega) \left\langle \frac{\delta B_n^2}{B_0^2} \right\rangle \left[\Omega - \Omega_*(\Omega) \right] \quad , \tag{3}$$

$$\mu_{\|\mathrm{P}}(\Omega) = \frac{0.21 |n| \mathrm{v}_{ti}^2 \sqrt{\epsilon \hat{\nu}}}{\langle R^2 \rangle \left[|\omega_E|^{3/2} + 0.30 |\omega_{\nabla B}| \sqrt{\hat{\nu}} + 0.04 \hat{\nu}^{3/2} \right]} \quad . \tag{4}$$

The details of the derivation can be found in Appendix A. The smoothed NTV offset frequency is

$$\Omega_*(\Omega) \equiv \frac{c_p + c_t(\Omega)}{Z_i e} \frac{dT_i}{d\chi} \quad , \tag{5}$$

$$c_t(\Omega) = \frac{2.84 \, |\omega_E|^{3/2} + 0.84 |\omega_{\nabla B}| \sqrt{\hat{\nu}} + 0.10 \hat{\nu}^{3/2}}{|\omega_E|^{3/2} + 0.34 |\omega_{\nabla B}| \sqrt{\hat{\nu}} + 0.02 \hat{\nu}^{3/2}} - \frac{5}{2} \quad . \tag{6}$$

Here $|\omega_E|$ should be expanded via Eq. (2), $\hat{\nu} \equiv \nu_i / (|n| \epsilon)$ for compactness, and n is the toroidal mode number of the applied non-axisymmetric field. The grad-B drift frequency for superbananas is $\omega_{\nabla B}$, estimated for thermal particles as $|\omega_{\nabla B}| \equiv T_j / (|Z_j e|) \, |d\epsilon / d\chi|$ [20]. For simplicity, we have taken only the very deep sbp regime, in the limit $E_r \to 0$, and thus eliminated any pitch-angle dependence on the toroidal precessional drift or the need for pitch-angle integrals. A more complete connection formula using the WKB method will be presented in a future publication. Shaing has provided a more complicated connection formula than that presented here, by performing Padé approximation within the pitch-angle and energy integrals [21]. The emphasis in this work is on the existence of an experimental peak in the NTV torque at low E_r (i.e., $|\omega_E| \to 0$), which is predicted by Eq. (3) and Eq. (4).

The Padé approximant damping rate $\mu_{\|\mathrm{p}}(\Omega)$ is a strongly peaked function of Ω around Ω_0, where $E_r \simeq 0$. Near this peak, Eq. (4) reduces to either the sbp regime for $\nu_i / (|n| \epsilon) < 7.5 \, |\omega_{\nabla B}|$ or the $1/\nu$ regime when the converse is true. Outside of the peaked region, Eq. (4) quickly transitions to the $\sqrt{\nu}$ regime. Integrating the flux-surface-averaged NTV damping rate over the plasma volume via $\int dV \, [\mathrm{Eq.}\,(3)] \, \langle R^2 \rangle \, \rho_M$ yields the total NTV torque on the plasma. In the large aspect-ratio limit this reduces to

$$-T_{NTV} = 4\pi^2 R_0^3 \int_0^a r dr \rho_M \mu_{\|\mathrm{P}}^{\mathrm{cyl}} \left\langle \frac{\delta B_n^2}{B_0^2} \right\rangle (\Omega - \Omega_*)^{\mathrm{cyl}} \quad . \tag{7}$$

Here the superscript "cyl" denotes we have approximated $\Omega \equiv \left\langle R^2 \vec{V} \cdot \vec{\nabla} \zeta \right\rangle / \langle R^2 \rangle \sim V_\zeta / R$ along the outboard midplane in what follows.

IV. EXPERIMENTAL METHOD

To investigate the existence of the peak in the total NTV torque predicted by the combination of Eqs. (4) and (7), non-axisymmetric magnetic field perturbations are applied to DIII-D plasmas using the I-coils: a set of 12 picture-frame coils toroidally distributed at two poloidal locations, six above and six below the midplane [18]. For this experiment, the I-coils are configured in "odd-parity" (the upper set of coils are out of phase with the lower set by 180°) to apply predominantly non-resonant $n = 3$ magnetic fields. The DIII-D plasmas presented in this paper are moderate $\beta_N \sim 1.6 - 1.7$, high confinement (H-mode) discharges, and have similar lower single null diverted cross sections. Typical ion density, ion temperature, and toroidal rotation profiles along the outboard midplane are shown in Fig. 2 plotted against a normalized minor radius ρ. (Here, $\rho \propto \sqrt{\Psi}$ such that $0 \leq \rho \leq 1$ across the plasma and Ψ is the toroidal magnetic flux).

The total NTV torque dependence on toroidal rotation is observed by making several plasmas with similar safety factor q, density, and temperature, but different toroidal rotation Ω. In each shot, the density, temperature, β_N, and toroidal rotation Ω (determined by a preprogrammed mix of co- and counter-I_p neutral beam injected (NBI) torque) are allowed to reach steady-state (Fig. 3). To measure the dependence of the radially integrated total NTV torque Eq. (7) on toroidal rotation the neutral beams are operated in rotation feedback mode, attempting to hold constant the observed charge exchange recombination (CER) carbon impurity rotation, Ω_C, at the $\rho = 0.67$ surface. While the beams are in rotation feedback, the I-coils are rapidly switched on at $t \simeq 2050$ ms to 3 kA. As is clear in Fig. 3, the neutral beams maintain the $\rho = 0.67$ impurity rotation value of $\Omega_C \simeq 10$ krad/s; but this requires $\Delta T_{NBI} \sim 1$ Nm *less* counter-I_p injected neutral beam torque after the I-coil $n = 3$ fields are applied. As shown in Fig. 2, the beam feedback successfully keeps the equilibrium profiles fixed at $\rho = 0.67$ (vertical dashed line).

The total NTV torque applied by the I-coils, i.e., that given by Eq. (7), can be read directly from the jump in the beam torque: $\Delta T_{NBI} = -T_{NTV}(\Omega)$ as seen in Fig. 3, which is calculated using TRANSP [22]. For this particular shot, 138574, the toroidal rotation rate at the $\rho = 0.67$ surface is $\Omega_C \simeq 10$ krad/s. This torque measurement procedure is repeated for several similar discharges, with different Ω_C values on the $\rho = 0.67$ surface. The resultant total NTV torque as a function of the deuterium toroidal rotation rate Ω (calculated from

Ω_C using NCLASS [23]) at the $\rho = 0.67$ surface is plotted with diamonds in Fig. 5 and clearly shows a peak. This is in contradiction with the NTV torque obtainable by neglecting any Ω (or E_r) dependence in the damping rate Eq. (4), which would produce a *linear* NTV torque with rotation rate, i.e., $-T_{NTV} \propto (\Omega - \Omega_*)$.

To compare the NTV torque predicted by Eq. (7) with the experimental data, the non-resonant magnetic perturbation profile $\langle \delta B_n^2(r)/B_0^2 \rangle$ from the applied $n = 3$ fields is calculated using the MARS-F [24] code and shown in Fig. 4 for both vacuum and plasma cases. Since the plasmas in this paper were moderate $\beta_N \sim 1.6 - 1.7$ and the I-coils were configured in "odd-parity" insuring non-pitch resonant perturbations were applied, the difference between vacuum and plasma δB is small. CER poloidal rotation data was unavailable for all but one of the shots. Thus direct measurement of E_r via (2) is not possible. Following the neoclassical flow damping arguments discussed earlier, we assume the poloidal flow is damped to $\left\langle q\vec{V}_i \cdot \vec{\nabla}\theta \right\rangle \simeq (c_p/Z_i e) dT_i/d\chi$ on the ion-ion collision timescale. Then, the radial electric field is completely determined by (2) which in the cylindrical limit reduces to

$$\omega_E^{\rm cyl} \simeq \frac{c_p - 1}{Z_i e}\left(\frac{dT_i}{d\chi}\right) - \frac{T_i}{Z_i e n_i}\left(\frac{dn_i}{d\chi}\right) - \Omega^{\rm cyl} \quad . \tag{8}$$

A theoretical NTV torque scan is performed with Eq. (7) using the equilibrium for shot 138574 at 2400 ms. The profiles are held fixed, while the deuterium toroidal rotation profile is scanned self-similarly, i.e., $\Omega(\rho) = \Omega f(\rho)$, where $-30 \le \Omega \le 15$ krad/s and $f(\rho) \equiv \Omega(\rho)/\Omega(0.67)$ is a normalized rotation profile from shot 138574 at 2400 ms. The computed torque as a function of Ω is shown by the solid line labeled "model" in Fig. 5. In addition, the NTV torque Eq. (7) is calculated for each shot independently and plotted (triangles) in the same figure. In all cases, the profiles are integrated from $\rho = 0.0$ to 0.95. The point NTV rotation scan (triangles) is calculated by taking the average of the computed torque profile ∼100 ms before and ∼400 ms after the I-coil switch-on.

V. RESULTS AND DISCUSSION

Reasonable agreement between the model (line), the theory points (triangles), and the data (diamonds) for the location of the peak center in Fig. 5 is obtained by fitting the unknown value of the equilibrium neoclassical poloidal rotation constant c_p to a value of $c_p = 1.4$. The width of the peak predicted by theory is narrower than the data by a

factor of 3. From a theoretical viewpoint, this is not surprising since we have used a Padé approximation between asymptotic regimes which does not smooth over pitch angle and particle energy.

Using NCLASS, we may estimate c_p using

$$c_p^{\rm NCLASS} \equiv c_p^N \simeq Z_i e\, U_{\theta,i}\, B_0^2\, (B_t R\, dT_i/d\chi)^{-1} \quad , \tag{9}$$

$U_{\theta,i} \equiv \vec{V}_i \cdot \vec{\nabla}\theta/(\vec{B} \cdot \vec{\nabla}\theta)$, and B_t is the toroidal component of the magnetic field. For shot 138574 at 2400 ms, Eq. (9) varies across the plasma minor radius with a mean value of $\overline{c_{pN}} = 0.7$ and produces a torque similar to the dashed curve plotted in the top panel of Fig. 6. However, our NTV model (7) is sensitive to variation in c_p, as it determines where in the minor radius $E_r = 0$. To illustrate this, we have calculated the NTV torque using Eq. (9) scaled by three different values of c_p at the $\rho = 0.67$ surface. The result is shown in the top panel of Fig. 6. In addition, we have calculated Eq. (7) using a *flat* c_p profile also scaled by three different values of c_p, shown in the top panel of Fig. 7. In both cases, values of c_p greater than the "best fit" value of 1.4 produce torque curves peaked to the left, or counter$-I_p$ direction of the experimental peak, and vice-versa for c_p values less than 1.4. Plotted in the lower panel of Fig. 6 through Fig. 7 are the location of the radial electric field roots along the minor radius versus toroidal rotation rate Ω (at $\rho = 0.67$) for each of the torque curves shown in the upper panel of the figures. The shape of the torque curves correlates well with the existence of E_r roots. Several electric field roots for a given rotation value lead to a local maxima in the NTV torque versus Ω. The most extreme example is shown in the "best-fit" $c_p = 1.4$ curve in Fig. 7, where there are several E_r roots between $\rho \simeq 0.65 - 0.9$ for $\Omega \simeq -2.5$ (krad/s) (i.e., the E_r-root curve is nearly vertical).

To estimate the sensitivity in determining c_p from our model, Eq. (7) is plotted against the data for three different choices of a flat c_p profile in the top plot of Fig. 8. The torque curve for the best fit value of $c_p = 1.4$ is well bracketed by the two curves with $c_p = 0.8$ and $c_p = 2.0$. Thus, the c_p^N values for $\rho > 0.7$ would place the NTV theory model peak beyond (in the co-I_p direction) the experimental data in the top panel of Fig. 8. The center panel in Fig. 8 shows a representative NTV torque density profile $t_{\rm NTV} \equiv dT_{NTV}/dV$ for $c_p = 1.4$. Local maxima (and one inflection point) exist approximately everywhere the radial electric field vanishes as determined by Eq. (8) and shown with ω_E in the lower panel in Fig. 8.

VI. SUMMARY

This paper reports the first observation of a theoretically-predicted peak in the NTV torque for low toroidal rotation rates, $-10 < \Omega < 5$ krad/s, in DIII-D by applying external $n = 3$ non-axisymmetric non-axisymmetric magnetic fields with the I-coils. The location of the experimental peak center agrees with a reduced NTV theory model when the poloidal rotation parameter is fitted to a value $c_p = 1.4$. This differs from the averaged value $\overline{c_{pN}} = 0.7$ predicted by axisymmetric neoclassical theory, by a factor of two. The observed width remains wider than the model by roughly a factor of 3. The reduced NTV model presented here is meant to illustrate the theoretical prediction of a peak NTV torque at low toroidal rotation. Further calculations with a more sophisticated NTV formula involving smoothed integrals in pitch angle and particle energy will be left to a future publication. These results are significant in demonstrating that the $\vec{E}\times\vec{B}$ and diamagnetic-level poloidal and toroidal flows and the torques on them discussed here and in Refs. [6, 17] are as predicted by a combination of axisymmetric and non-axisymmetric neoclassical theory. NTV has the potential to alter rotation profiles in low external torque configurations for a variety of applications in ITER.

Acknowledgment

This research was supported by the U.S. Department of Energy under DE-FG02-86ER53218, DE-FG02-92ER54139, DE-FG02-99ER54546, DE-FC02-04ER54968, DE-FG02-89ER53297 and DE-AC02-09CH11466. Figures were generated using Scilab ®: `http://www.scilab.org`.

APPENDIX A: DERIVATION OF NTV TORQUE MODEL

In this appendix we derive Eq. (3) from the various asymptotic collisionality regimes calculated by K.C. Shaing in Hamada coordinates. In what follows we employ straight-field-line Clebsch coordinates where $\vec{B} = \vec{\nabla}\chi \times \vec{\nabla}\left(q\theta - \zeta\right)$, with (χ, θ, ζ) being the poloidal flux over 2π, and θ (ζ) a poloidal (toroidal) angle. For simplicity, consider a model up/down symmetric tokamak field, whose magnetic field magnitude in the presence of field errors may

be decomposed as

$$B = B_0(\theta) + \sum_{m,n} b_{nm} e^{i\alpha_{m,n}} \quad , \tag{A1}$$

$$B_0(\theta) = B_0 \left(1 - \epsilon \cos\theta\right), \qquad \epsilon = r/R_0 \quad , \tag{A2}$$

where the m, n helical angle is defined as $\alpha_{m,n} \equiv m\theta - n\zeta$, and the harmonic coefficients satisfy $|b_{nm}|/B_0 \ll \epsilon$.

We make two simplifying approximations from Shaing's original derivation after mapping to general (χ, θ, ζ) coordinates. *Firstly*, we neglect the coordinate Jacobian $(1/\vec{B} \cdot \vec{\nabla}\theta)$ in determining the kinetic integrals giving the regime-dependent numerical NTV damping rate and offset frequency (effectively we are computing the Hamada coordinate numbers); *secondly*, the damping rate and offset frequency in general contain integrals over the perturbed magnetic field spectrum whose differences we will neglect. We simplify the dependence on the perturbed magnetic field as follows. In each NTV regime to be smoothly connected in this work, the torque density on the plasma depends upon the perturbed magnetic field spectrum as

$$t_{\rm NTV} \propto -\mu_{\parallel}(\nu_i, E_r) \left\langle \frac{\delta B^2}{B_0^2} \right\rangle^{\rm eff} \quad , \tag{A3}$$

where in general

$$\left\langle \frac{\delta B^2}{B_0^2} \right\rangle^{\rm eff} = \sum_n \sum_{mm'} \frac{b_{mn} b_{m'n}^*}{B_0^2} \int_0^1 d\kappa^2 f_{mn}(\kappa^2) f_{m'n}(\kappa^2) \quad , \tag{A4}$$

$$f_{mn}(\kappa^2) \propto \oint \frac{d\theta}{\vec{B} \cdot \vec{\nabla}\theta} \left[v_{\parallel}/v\right]^{\gamma} \cos\left(\Delta_{mn}\right) \quad . \tag{A5}$$

The integration variable κ^2 is a frequently-used, normalized pitch-angle variable ranging from $\kappa^2 = 0$ (deeply trapped) to $\kappa^2 = 1$ (trapped-passing boundary), and given by

$$\kappa^2 = \frac{1 - \lambda + \lambda\epsilon}{2\lambda\epsilon} \quad , \tag{A6}$$

$$\lambda = \frac{\mu B_0}{\frac{1}{2} m_j v^2} \equiv \frac{\mu B_0}{\mathcal{E}} \quad . \tag{A7}$$

Here μ is the usual magnetic moment, $\Delta_{mn} \equiv (m - nq)\theta$, and the exponent γ depends on NTV regime. The θ integrals are over an (up-down symmetric) equilibrium bounce orbit: $\oint d\theta \equiv \int_{-\theta_t}^{+\theta_t}$, with $\theta_t = 2\arcsin(\kappa)$. We normalize the pitch-angle integral in each regime such that

$$\left\langle \frac{\delta B^2}{B_0^2} \right\rangle^{\rm eff} = \sum_n \sum_{mm'} \frac{b_{mn} b_{m'n}^*}{B_0^2} \int_0^1 \frac{d\kappa^2}{A_\gamma} f_{mn}(\kappa^2) f_{m'n}(\kappa^2) \quad , \tag{A8}$$

where

$$A_\gamma \equiv \int_0^1 d\kappa^2 \left[f_{m=nq,n}(\kappa^2) \right]^2 \quad . \tag{A9}$$

In this way, the set of f_{mn} with the least oscillatory integrand over a bounce orbit result in a pitch-angle integral equal to unity. The numerical coefficient A_γ is absorbed in the damping rate $\mu_\parallel$ for each regime, and we hereafter approximate

$$\left\langle \frac{\delta B^2}{B_0^2} \right\rangle^{\text{eff}} \simeq \sum_n \sum_{mm'} \frac{b_{mn} b^*_{m'n}}{B_0^2} \tag{A10}$$

in each NTV regime to be smoothly connected in the torque model.

1. Low collisionality $1/\nu$ regime

A detailed derivation of K.C. Shaing's $1/\nu$ NTV regime torque in terms of flows instead of thermodynamic forces and in general (χ, θ, ζ) coordinates can be found in Sec. III of Ref. [25]. (Shaing's original derivation is published in Ref. [2].) The flux-surface-averaged NTV torque density for species j in the $1/\nu$ regime is (Eq. (49) in Ref. [25]):

$$t_{j,1/\nu} = -\left\langle \vec{e}_\zeta \cdot \vec{\nabla} \cdot \overleftrightarrow{\Pi}_j \right\rangle = -n_j m_j \mu_{\parallel j}^{1/\nu} \left\langle \left(\frac{\delta B_n^{1/\nu}}{B_0} \right)^2 \right\rangle \times \left(\left\langle R^2 \vec{V}_j \cdot \vec{\nabla} \zeta \right\rangle - \left\langle R^2 \Omega_{*j}^{1/\nu} \right\rangle \right) \quad , \tag{A11}$$

where the damping rate and offset rotation are respectively

$$\mu_{\parallel j}^{1/\nu} = \sqrt{\frac{2}{\pi^3}} \, \lambda_{j;1} \, \epsilon^{3/2} \frac{\mathrm{v}_{tj}^2}{\langle R^2 \rangle \, \nu_j} \quad , \tag{A12}$$

$$\left\langle R^2 \Omega_{*j}^{1/\nu} \right\rangle = \left\langle R^2 q \vec{V}_j \cdot \vec{\nabla} \theta \right\rangle + \frac{c_{t,j}^{1/\nu}}{Z_j e} \frac{dT_j}{d\chi} \left\langle R^2 \right\rangle ,$$

$$\simeq \frac{c_{p,j} + c_{t,j}^{1/\nu}}{Z_j e} \frac{dT_j}{d\chi} \left\langle R^2 \right\rangle \quad . \tag{A13}$$

The kinetic integrals over normalized particle kinetic energy $x = \mathcal{E}_j / T_j$ appearing above are given by

$$\lambda_{j;1} = \frac{4\pi^2 \mathcal{J}}{A} \frac{1}{2} \int_0^\infty \frac{e^{-x} \, x^4 \, dx}{F(x; b_j)} \quad , \tag{A14}$$

$$\lambda_{j;2} = \frac{4\pi^2 \mathcal{J}}{A} \frac{1}{2} \int_0^\infty \frac{e^{-x} \, x^4 (x - 5/2) \, dx}{F(x; b_j)} \quad , \tag{A15}$$

where the flux surface area A and energy dependence of the perpendicular scattering operator $F(x;b_j)$ are defined by Eqs. (31) and (23) in [25] respectively. The numerical factor $\not{J}$ is determined by the normalization procedure discussed in Eqs. (A4)-(A9) and is

$$\not{J} \equiv \frac{4}{\left\langle \vec{B}\cdot\vec{\nabla}\theta \right\rangle}\int_0^1 d\kappa^2 \left[E(\kappa)-(1-\kappa^2)K(\kappa)\right] \quad , \\ = \frac{16}{9}\frac{A}{4\pi^2} \quad . \tag{A16}$$

Here the complete elliptic integrals of the first $[K(\kappa)]$ and second $[E(\kappa)]$ kind are defined in Ref. [26] and the modulus k given therein is our pitch-angle parameter κ. Thus our kinetic integrals (A14)–(A15) differ from those defined by Shaing (sentence following Eq. (17) in [2]) by a factor of 16/9. The $1/\nu$ regime toroidal rotation coefficient is $c_{t,j}^{1/\nu} \equiv \lambda_{j;2}/\lambda_{j;1}$. The effective perturbed magnetic field strength (squared) and associated integrals are

$$\left\langle \left(\frac{\delta B_n^{1/\nu}}{B_0}\right)^2 \right\rangle \equiv \sum_n n^2 \sum_{mm'} \frac{b_{nm}b_{nm'}^*}{B_0^2} \times \\ \int_0^1 d\kappa^2 \frac{J_{nm}(\kappa^2)J_{nm'}(\kappa^2)}{\not{J}\, J(\kappa^2)} \quad , \tag{A17}$$

$$J_{nm}(\kappa^2) \equiv \oint \frac{d\theta}{\vec{B}\cdot\vec{\nabla}\theta}\sqrt{\kappa^2-\sin^2(\theta/2)}\,\cos\Delta_{mn} \quad , \tag{A18}$$

$$J(\kappa^2) \equiv \oint \frac{d\theta}{\vec{B}\cdot\vec{\nabla}\theta}\sqrt{\kappa^2-\sin^2(\theta/2)} \quad . \tag{A19}$$

Henceforth we simplify the effective perturbed magnetic field strength in the $1/\nu$ regime to

$$\left\langle \left(\frac{\delta B_n^{1/\nu}}{B_0}\right)^2 \right\rangle \simeq \sum_n n^2 \sum_{mm'} \frac{b_{nm}b_{nm'}^*}{B_0^2} \quad . \tag{A20}$$

For ions in an electron-ion plasma, and neglecting $\vec{B}\cdot\vec{\nabla}\theta$ in the kinetic integrals, we find the damping rate and rotation offset are

$$\mu_{\|i}^{1/\nu} = 6.01\,\epsilon^{3/2}\frac{\mathrm{v}_{ti}^2}{\langle R^2\rangle\,\nu_i} \quad , \tag{A21}$$

$$\left\langle R^2\Omega_{*i}^{1/\nu}\right\rangle = \frac{c_{p,i}+2.36}{Z_i e}\frac{dT_i}{d\chi}\left\langle R^2\right\rangle \quad . \tag{A22}$$

2. $\sqrt{\nu}$-boundary layer

As the effective species collisionality $\nu_{\mathrm{eff}} = \nu_j/\left(|n|\epsilon\right)$ decreases, two effects can limit the radial transport/toroidal torque on the plasma. The first is a collisional boundary layer at the

trapped-passing boundary ($\kappa = 1$) which occurs when $\nu_{\rm eff} \ll \dot{\zeta}_0$, where $\dot{\zeta}_0 = \omega_E + \omega_{\vec{\nabla} B}$ is the trapped particle toroidal precession frequency [19]. The second effect involves a resonance in $\dot{\zeta}_0$ and is discussed in the next subsection. In terms of flows instead of thermodynamic forces and in general (χ, θ, ζ) coordinates, the boundary layer toroidal viscous force is

$$t_{j,\sqrt{\nu}} = -m_j n_j \mu_{\|j}^{\sqrt{\nu}} \left\langle \left(\frac{\delta B_n^{\sqrt{\nu}}}{B_0} \right)^2 \right\rangle \times \left(\left\langle R^2 \vec{V} \cdot \vec{\nabla} \zeta \right\rangle - \left\langle R^2 \Omega_{*j}^{\sqrt{\nu}} \right\rangle \right) \quad , \tag{A23}$$

where the damping rate and rotation offset are

$$\mu_{\|j}^{\sqrt{\nu}} \equiv \frac{w_{j;1}}{4\pi^{3/2}} \frac{\mathrm{v}_{tj}^2 \sqrt{\nu_j}}{\langle R^2 \rangle \, |\phi'|^{3/2}} \quad , \tag{A24}$$

$$\begin{aligned} \left\langle R^2 \Omega_{*j}^{\sqrt{\nu}} \right\rangle &\equiv \left\langle R^2 q \vec{V}_j \cdot \vec{\nabla} \theta \right\rangle + \frac{w_{j;2}}{w_{j;1}} \frac{\langle R^2 \rangle}{Z_j e} \frac{dT_j}{d\chi} \quad , \\ &\simeq \frac{c_{p,j} + c_{t,j}^{\sqrt{\nu}}}{Z_j e} \frac{dT_j}{d\chi} \langle R^2 \rangle \quad . \end{aligned} \tag{A25}$$

The $\sqrt{\nu}$ regime toroidal rotation coefficient is $c_{t,j}^{\sqrt{\nu}} \equiv w_{j;2}/w_{j;1}$. The kinetic coefficients appearing above are

$$\begin{aligned} w_{j;1} &\equiv \tau(\kappa_\delta) \sqrt{\frac{J(\kappa_\delta)}{\tau(\kappa_\delta)}} \frac{4\pi^2}{A} \frac{1}{2} \int_0^\infty dx e^{-x} x^{7/4} \sqrt{F(x; b_j)} \quad , \\ &\equiv \tau(\kappa_\delta) \sqrt{\frac{J(\kappa_\delta)}{\tau(\kappa_\delta)}} \frac{4\pi^2}{A} \hat{w}_{j;1} \quad , \end{aligned} \tag{A26}$$

$$\begin{aligned} w_{j;2} &\equiv \ldots \frac{1}{2} \int_0^\infty dx e^{-x} x^{7/4} \sqrt{F(x; b_j)} \left(x - \frac{5}{2} \right) \quad , \\ &\equiv \ldots \hat{w}_{j;2} \quad . \end{aligned} \tag{A27}$$

Here κ_δ is the pitch-angle variable evaluated at the edge of the boundary-layer, which is in general a function of both radial electric field and particle energy [Eq. (14) in [19]]. For simplicity, we fix $\kappa_\delta \simeq 0.89$ in this work. Both kinetic integrals appearing above have the same factor appearing in front of the integral as indicated with $(\ldots)$ for brevity. The normalized bounce time is

$$\tau(\kappa) = \oint \frac{d\theta}{\vec{B} \cdot \vec{\nabla} \theta} \frac{B/B_0}{\sqrt{\kappa^2 - \sin^2(\theta/2)}} \simeq \frac{4K(\kappa)}{\left\langle \vec{B} \cdot \vec{\nabla} \theta \right\rangle} \quad , \tag{A28}$$

where the last approximation is consistent with the discussion in the paragraph prior to (A3). The effective perturbed magnetic field in the $\sqrt{\nu}$ regime is

$$\left\langle \left(\frac{\delta B_n^{\sqrt{\nu}}}{B_0} \right)^2 \right\rangle \equiv \sum_n \sqrt{n} \sum_{mm'} \frac{b_{nm} b_{nm'}^*}{B_0^2} \frac{F_{nm}(\kappa_\delta) F_{nm'}(\kappa_\delta)}{\tau^2(\kappa_\delta)} \quad , \tag{A29}$$

$$\simeq \sum_n \sqrt{n} \sum_{mm'} \frac{b_{nm} b_{nm'}^*}{B_0^2} \quad , \tag{A30}$$

$$F_{mn}(\kappa) \equiv \oint \frac{d\theta}{\vec{B} \cdot \vec{\nabla}\theta} \frac{\cos \Delta_{mn}}{\sqrt{\kappa^2 - \sin^2(\theta/2)}} \quad . \tag{A31}$$

For ions in an electron-ion plasma, and neglecting $\vec{B} \cdot \vec{\nabla}\theta$ in the kinetic integrals, we find the damping rate and rotation offset are (Table A.I)

$$\mu_{\|i}^{\sqrt{\nu}} \simeq 0.13 K(\kappa_\delta) \frac{\mathrm{v}_{ti}^2 \sqrt{\nu_i}}{\langle R^2 \rangle \, |\phi'|^{3/2}} \quad , \tag{A32}$$

$$\left\langle R^2 \Omega_{*i}^{\sqrt{\nu}} \right\rangle \simeq \frac{c_{p,i} + 0.36}{Z_i e} \frac{dT_i}{d\chi} \langle R^2 \rangle \quad . \tag{A33}$$

3. Superbanana plateau regime

When $\nu_{\rm eff} \ll \dot{\zeta}_0$ and the radial electric field becomes small enough that the electric precessional drift is of the order of the magnetic precessional drift, resonances in the toroidal precessional drift can occur, i.e. $\omega_E = \omega_{\vec{\nabla}B}$. Under these conditions, a resonant plateau regime emerges which dominates the neoclassical toroidal viscosity [20]. Deep in this regime, in the limit that the radial electric field vanishes, the torque expression and kinetic coefficients are somewhat simplified. Thus, for our model torque equation we consider only the deep SBP limit where $E_r \to 0$. In terms of flows instead of thermodynamic forces and in general (χ, θ, ζ) coordinates, the sbp toroidal viscous force (Eq. (35) in Ref. [20]) is

$$t_{j,\rm sbp} = -\eta_1 \sqrt{\frac{\epsilon}{2\pi}} \frac{m_j n_j \mathrm{v}_{tj}^2}{\langle R^2 \rangle \, |\omega_{\nabla B}|} \left\langle \left(\frac{\delta B_n^{\rm sbp}}{B_0} \right)^2 \right\rangle \times \left[\left\langle R^2 \vec{V}_j \cdot \vec{\nabla}\zeta \right\rangle - \left\langle R^2 \Omega_{*j}^{\rm sbp} \right\rangle \right] \quad . \tag{A34}$$

Here the effective perturbed magnetic field is

$$\left\langle \left(\frac{\delta B_n^{\rm sbp}}{B_0} \right)^2 \right\rangle \equiv \sum_n |n| \sum_{mm'} \frac{b_{nm} b_{nm'}^*}{B_0^2} \frac{F_{nm}(\kappa_0) F_{nm'}(\kappa_0)}{\tau^2(\kappa_0)} \quad , \tag{A35}$$

which we approximate as

$$\simeq \sum_n |n| \sum_{mm'} \frac{b_{nm} b_{nm'}^*}{B_0^2} \quad . \tag{A36}$$

The kinetic coefficients deep in this regime are

$$\eta_1 \equiv \Gamma(5/2)\tau(\kappa_0)\kappa_0^2\left(1-\kappa_0^2\right)\frac{4\pi^2}{A} \simeq 1.773 \quad , \tag{A37}$$

while the second kinetic coefficient η_2 (proportional to c_t) is identically zero. Here $\kappa_0 \simeq 0.9089$ is the resonant pitch angle for which $\omega_{\vec{\nabla}B} = 0$, and η_1 is for both ions and electrons [20]. The numerical value at the end of Eq. (A37) neglects the variation of $\vec{B}\cdot\vec{\nabla}\theta$ in the θ integration. The $\vec{\nabla}B$ drift frequency estimated for non-resonant superbanana particles [20] and the offset rotation rate are respectively

$$|\omega_{\vec{\nabla}B,j}| \equiv \frac{1}{2}\frac{m_j \mathrm{v}_{tj}^2}{|Z_j e|}\left|\frac{d\epsilon}{d\chi}\right| \quad , \tag{A38}$$

$$\left\langle R^2\Omega_{*j}^{\mathrm{sbp}}\right\rangle \equiv \frac{c_{p,j}}{Z_j e}\frac{dT_j}{d\chi}\left\langle R^2\right\rangle \quad . \tag{A39}$$

For ions we find (A34) reduces to

$$t_{i,\mathrm{sbp}} = -m_i n_i \mu_{\|i}^{\mathrm{sbp}}\left\langle\left(\frac{\delta B_n^{\mathrm{sbp}}}{B_0}\right)^2\right\rangle \times \left[\left\langle R^2\vec{V}_i\cdot\vec{\nabla}\zeta\right\rangle - \left\langle R^2\Omega_{*i}^{\mathrm{sbp}}\right\rangle\right] \quad , \tag{A40}$$

where the damping rate is

$$\mu_{\|i}^{\mathrm{sbp}} \simeq 0.71\frac{\sqrt{\epsilon}\mathrm{v}_{ti}^2}{\left\langle R^2\right\rangle|\omega_{\vec{\nabla}B,i}|} \quad . \tag{A41}$$

4. Padé connection formula

All of the regimes in this paper diverge outside of the their region of applicability in ν_i, ω_E parameter space. While there is no unique method to connect them, a simple way to construct a damping rate $\mu_\|$ which smoothly transitions between all the asymptotic regimes is by inverse addition:

$$\frac{1}{\mu_{\mathrm{tot}}} = \sum_l \frac{1}{\mu_l} \quad , \tag{A42}$$

where the index refers to asymptotic regimes, i.e. $l = 1$ might be $1/\nu$, $l = 2$ sbp, and so on. Making the dependence on the toroidal mode number n explicit and summing over mode

numbers we have a smoothed torque model for species j of the form

$$t_{j,NTV} = -\sum_n m_j n_j \sum_{m,m'} \frac{b_{nm} b^*_{nm'}}{B_0^2} \mu_{j;1\,S}(n) \times \left[\left\langle R^2 \vec{V}_j \cdot \vec{\nabla}\zeta \right\rangle - \Omega_{*j,S} \right], \tag{A43}$$

$$\Omega_{*j,S} \equiv \frac{c_{p,j} + c_{t,j}(n)}{Z_j e} \frac{dT_j}{d\chi} \left\langle R^2 \right\rangle \quad . \tag{A44}$$

Here the smoothed viscous coefficients connecting between the various regimes are

$$\mu_{j;k\,S}(n) \equiv \frac{(\mathrm{v}_{tj})^2}{\langle R^2 \rangle} \frac{\lambda^{\mathrm{sq}}_{j;k} \sqrt{\nu_j} \sqrt{|n|}}{A_{j;k} + |\omega_E|^{3/2}} \qquad k = 1, 3 \quad , \tag{A45}$$

$$A_{j;k} \equiv \frac{\lambda^{\mathrm{sq}}_{j;k}}{\lambda^{\mathrm{sbp}}_{j;k}} \left| \omega_{\vec{\nabla}B,j} \right| \sqrt{\frac{\nu_j}{|n|\epsilon}} + \frac{\lambda^{\mathrm{sq}}_{j;k}}{\lambda^{1/\nu}_{j;k}} \left(\frac{\nu_j}{|n|\epsilon} \right)^{3/2} \quad . \tag{A46}$$

The toroidal rotation coefficient vanishes in the sbp regime and the inverse addition method Eq. (A42) fails. However, the numerical viscous coefficients are in general given by

$$\lambda_1 = \int_0^\infty dx\, e^{-x} f(x) \quad , \tag{A47}$$

$$\lambda_2 = \int_0^\infty dx\, e^{-x} f(x) \left(x - \frac{5}{2} \right) \equiv \lambda_3 - \frac{5}{2} \lambda_1 \quad , \tag{A48}$$

where the integration is over normalized particle energy $x = \mathcal{E}_j / T_j$, and the details of $f(x)$ depend on the NTV regime. Therefore, we can smoothly patch λ_1 and λ_3 independently via (A42), as neither one vanishes in any collisionality regime presented in this work. The result of this is the patched toroidal rotation coefficient,

$$c_{t,j}(n) \equiv \frac{\mu_{j;3\,S}(n)}{\mu_{j;1\,S}(n)} - \frac{5}{2} = \frac{\lambda^{\mathrm{sq}}_{j;3}}{\lambda^{\mathrm{sq}}_{j;1}} \frac{A_{j;1} + |\omega_E|^{3/2}}{A_{j;3} + |\omega_E|^{3/2}} - \frac{5}{2}, \tag{A49}$$

which being a ratio of smoothed functions is less significant in its variation than the damping rate Eq. (A45) but is listed here for completeness. In light of this redefinition, we list the

numerical coefficients defined in the preceding equations:

$$\lambda_{j;k}^{\rm sbp} \equiv \frac{\eta_k}{\sqrt{2\pi}} \equiv \frac{\tau(\kappa_0)}{\sqrt{2\pi}}\kappa_0^2\left(1-\kappa_0^2\right)\frac{4\pi^2}{A}\times \begin{cases} \Gamma(5/2) \text{ for } k=1 \\ \Gamma(7/2) \text{ for } k=3 \end{cases} , \tag{A50}$$

$$\lambda_{j;k}^{\rm sq} \equiv \frac{w_{j;k}}{4\pi^{3/2}} = \sqrt{\frac{J(\kappa_\delta)}{\tau(\kappa_\delta)}}\frac{\tau(\kappa_\delta)}{4\pi^{3/2}}\frac{4\pi^2}{A}\hat{w}_{j;k} \quad , \\ \simeq \sqrt{E(\sqrt{\kappa_\delta})K(\sqrt{\kappa_\delta})}\frac{\hat{w}_{j;k}}{\pi^{3/2}} \quad , \tag{A51}$$

$$\lambda_{j;k}^{1/\nu} \equiv \sqrt{\frac{2}{\pi^3}}\lambda_{j;k} \quad . \tag{A52}$$

The $1/\nu$ kinetic coefficients $\lambda_{j;k}$ in Eq. (A52) are defined in Eqs. (A14) through (A15). The third kinetic coefficients for the $\sqrt{\nu}$ and $1/\nu$ regimes are respectively

$$\hat{w}_{j;3} \equiv \frac{1}{2}\int_0^\infty dx e^{-x}x^{11/4}\sqrt{F(x;b_j)} \quad , \tag{A53}$$

$$\lambda_{j;3} \equiv \frac{4\pi^2\mathcal{J}}{A}\frac{1}{2}\int_0^\infty \frac{e^{-x}\,x^5\,dx}{F(x;b_j)} = \frac{8}{9}\int_0^\infty \frac{e^{-x}\,x^5\,dx}{F(x;b_j)} \quad . \tag{A54}$$

Restricting the above equations to a single m,n perturbation yields Eq. (3) through (6).

[1] J. Luxon, M. Schaffer, G. Jackson, J. Leuer, A. Nagy, J. Scoville, and E. Strait, Nucl. Fusion **43**, 1813 (2003).

[2] K. C. Shaing, Phys. Plasmas **10**, 1443 (2003).

[3] J. D. Callen, Nucl. Fusion (2011), in publication.

[4] E. Lazzaro, R. J. Buttery, T. C. Hender, P. Zanca, R. Fitzpatrick, M. Bigi, T. Bolzonella, R. Coelho, M. DeBenedetti, S. Nowak, et al. (Contributors to the EFDA-JET work programme), Phys. Plasmas **9**, 3906 (2002).

[5] W. Zhu, S. A. Sabbagh, R. E. Bell, J. M. Bialek, M. G. Bell, B. P. LeBlanc, S. M. Kaye, F. M. Levinton, J. E. Menard, K. C. Shaing, et al., Phys. Rev. Lett. **96**, 225002 (2006).

[6] A. M. Garofalo, K. H. Burrell, J. C. DeBoo, J. S. deGrassie, G. L. Jackson, M. Lanctot, H. Reimerdes, M. J. Schaffer, W. M. Solomon, and E. J. Strait, Phys. Rev. Lett. **101**, 195005 (2008).

[7] R. J. La Haye, S. Günter, D. A. Humphreys, J. Lohr, T. C. Luce, M. E. Maraschek, C. C. Petty, R. Prater, J. T. Scoville, and E. J. Strait, Phys. Plasmas **9**, 2051 (2002), see p. 2058.

[8] S. P. Gerhardt, J. E. Menard, J.-K. Park, R. Bell, D. A. Gates, B. P. L. Blanc, S. A. Sabbagh, and H. Yuh, Plasma Phys. and Control. Fusion **52**, 104003 (2010).

[9] R. Aymar, V. A. Chuyanov, M. Huguet, Y. Shimomura, I. J. C. Team, and I. H. Teams, Nucl. Fusion **41**, 1301 (2001).

[10] K. C. Shaing and J. D. Callen, Phys. Fluids **26**, 3315 (1983).

[11] J. D. Callen, A. J. Cole, and C. C. Hegna, Nucl. Fusion **49**, 085021 (2009).

[12] J. D. Callen, A. J. Cole, and C. C. Hegna, Phys. Plasmas **16**, 082504 (2009).

[13] F. L. Hinton and R. D. Hazeltine, Rev. Mod. Phys. **48**, 239 (1976).

[14] A. J. Cole, C. C. Hegna, and J. D. Callen, Phys. Rev. Lett. **99**, 065001 (2007).

[15] A. J. Cole, C. C. Hegna, and J. D. Callen, Phys. Plasmas **15**, 056102 (2008).

[16] M.-D. Hua, I. T. Chapman, A. R. Field, R. J. Hastie, S. D. Pinches, and the MAST Team, Plasma Phys. and Control. Fusion **52**, 035009 (2010).

[17] A. M. Garofalo, W. M. Solomon, M. Lanctot, K. H. Burrell, J. C. DeBoo, J. S. deGrassie, G. L. Jackson, J.-K. Park, H. Reimerdes, M. J. Schaffer, et al., Phys. Plasmas **16**, 056119 (2009).

[18] G. L. Jackson, P. M. Anderson, J. Bialek, W. P. Cary, G. L. Campbell, A. M. Garofalo, R. Hatcher, A. G. Kellman, R. J. LaHaye, A. Nagy, et al., in *Proceedings of the 30th EPS Conference on Controlled Fusion Plasma Physics, St. Petersburg, Russia*, edited by R. Koch and S. Lebedev (European Physical Society, Petit-Lancy, 2003), Europhysics Conference Abstracts, contributed papers,Vol. 27A, p. P-4.47 on CD-ROM.

[19] K. C. Shaing, P. Cahyna, M. Becoulet, J.-K. Park, S. A. Sabbagh, and M. S. Chu, Phys. Plasmas **15**, 082506 (2008).

[20] K. C. Shaing, S. A. Sabbagh, and M. S. Chu, Plasma Phys. and Cont. Fusion **51**, 035009 (2009).

[21] K. Shaing, S. Sabbagh, and M. Chu, Nucl. Fusion **50**, 025022 (2010).

[22] R. Hawryluk, in *Phys. of Plas. Close to Thermo. Cond.*, edited by B. Coppi et al. (CEC, Brussels, 1980), p. 19.

[23] W. A. Houlberg, K. C. Shaing, S. P. Hirshman, and M. C. Zarnstorff, Phys. Plasmas **4**, 3230 (1997).

[24] Y. Q. Liu, A. Bondeson, C. M. Fransson, B. Lennartson, and C. Breitholtz, Phys. Plasmas **7**, 3681 (2000).

[25] A. J. Cole, C. C. Hegna, and J. D. Callen, Tech. Rep. UW-CPTC 08-8, University of Wisconsin, http://www.cptc.wisc.edu (2009).

[26] M. Abramowitz and I. A. Stegun, *Handbook of Mathematical Functions with Formulas, Graphs, and Mathematical Tables* (Dover, New York, 1964), 9th ed., ISBN 0-486-61272-4.

TABLE I: Kinetic coefficients for deuterium/electron plasma with mass ratios $b_i = 1/3672$ and $b_e = 3672$ in the $\sqrt{\nu}$ boundary layer.

	$\hat{w}_1$	$\hat{w}_2$
Ions	0.72	0.26
Electrons	1.07	0.32

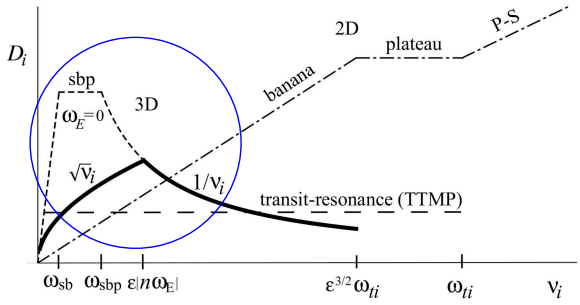

FIG. 1: (Color online) Key (circled region) ion diffusivities induced by variation in $|B|$ versus ion collision frequency [3]. The relevant non-axisymmetric diffusivities which drive a flux-surface-averaged toroidal viscous force density, i.e., $\left\langle \vec{e}_\zeta \cdot \vec{\nabla} \cdot \overleftrightarrow{\pi}_\parallel \right\rangle$ are labeled "3D". The regimes which lead to large radial ion diffusivities and large toroidal viscosity are the $1/\nu$, superbanana-plateau (sbp), and $\sqrt{\nu}$. For reference, the familiar axisymmetric regimes responsible for *parallel* to $\vec{B}$ flow damping, i.e. $\left\langle \vec{B} \cdot \vec{\nabla} \cdot \overleftrightarrow{\pi}_\parallel \right\rangle$, are labeled "2D" and they are: the banana, plateau, and Pfirsch-Schlüter (PS) regimes.

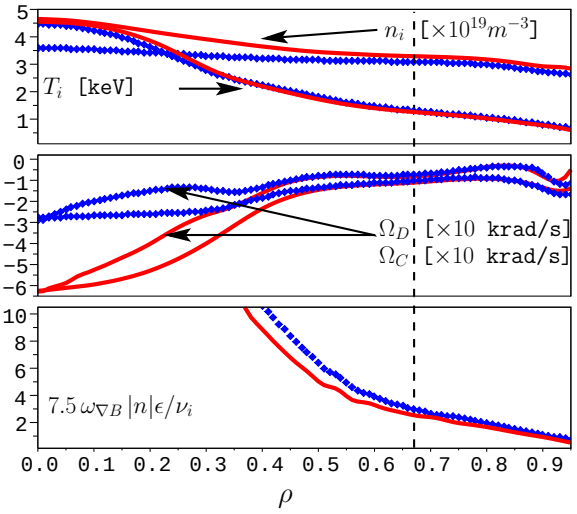

FIG. 2: (Color online) Experimental profiles (a,b) for shot 138574 at $t = 1900$ ms (solid line) and $t = 2400$ ms (marker). Vertical dashed line shows surface where CER feedback was performed. (c) Plot indicating $\nu_i/(|n|\epsilon) < 7.5|\omega_{\nabla B}|$, peak NTV torque in core governed by the sbp regime [20]. As $\rho \to 1$ the sbp and $1/\nu$ [2] regimes become comparable in this model, (i.e., as the ratio approaches unity).

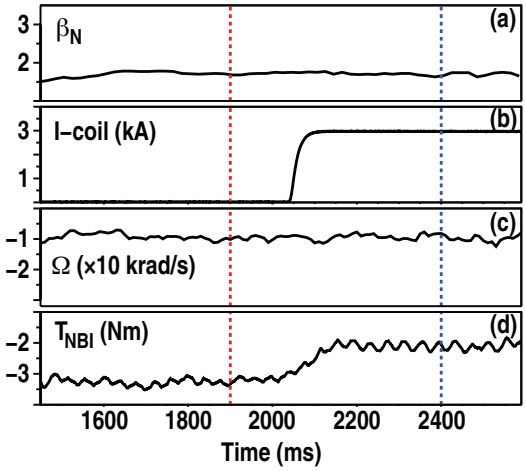

FIG. 3: (Color online) Experimental time trace for shot 138574, showing β_N, I-coil current, rotation rate at $\rho = 0.67$, and the total injected neutral beam torque. Positive rotation and NBI torque are both in the co-I_p direction. Vertical dashed lines refer to the profiles plotted in Fig. 2 before ($t = 1900$ ms) and after ($t = 2400$ ms) I-coil switch-on.

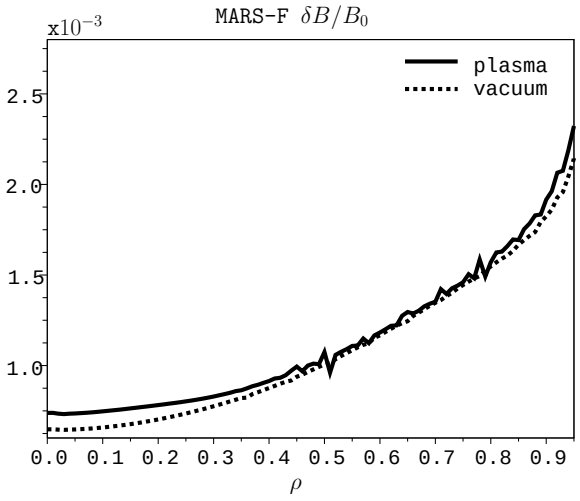

FIG. 4: MARS-F flux surface averaged $\delta B/B_0 \equiv \sqrt{\langle \sum_{mn} \delta B_{mn}^2 \rangle}/B_0$ normalized to the toroidal field on the magnetic axis ($B_0 = 1.92$ Tesla). Profiles are plotted versus normalized minor radius ρ, at 2405 milliseconds for shot 138574 with 3 kA applied to the I-coils. Note the modest difference between plasma and vacuum calculations. Only the plasma profile is used in this paper.

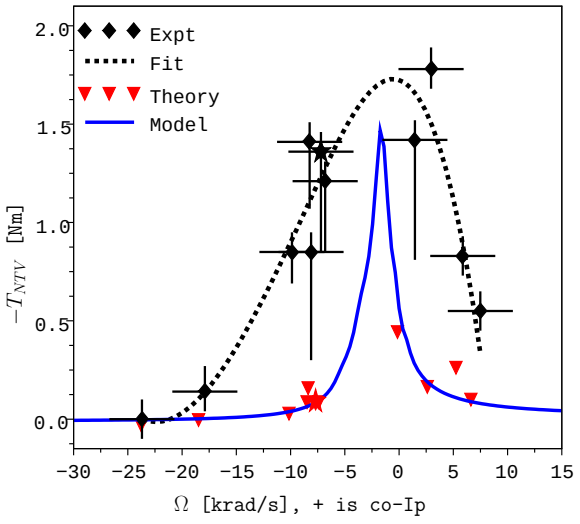

FIG. 5: (Color online) Comparison of measured NTV (diamonds), and cylindrical torque model (line) versus deuterium toroidal rotation (obtained from NCLASS) at $\rho = 0.67$. A least-squares spline fit (dashed) is shown for the data. Individual NTV torque points (triangles) are shown for each shot by taking the average of (7) computed slightly before and after I-coil switch-on. The starred points indicate shot 138574.

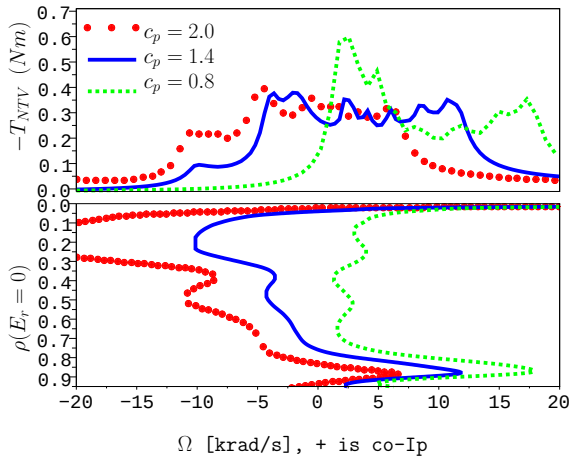

FIG. 6: (Color online) Total cylindrical $(m, n = 2, 3)$ NTV torque (a) with E_r roots determined using NCLASS c_p profiles, with scaled amplitude as indicated in the key. (b) Location of radial electric field roots along minor radius for each torque curve in (a). The self-similar nature of the NCLASS torque peaks is easily understood by the persistent, semi-stationary E_r root at $\rho \simeq 0.8 - 0.85$.

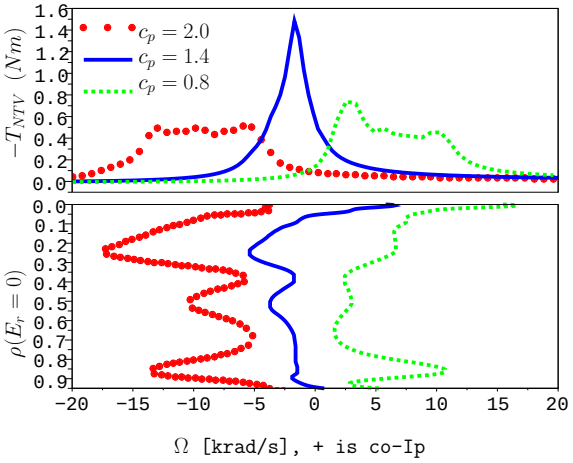

FIG. 7: (color online) Total cylindrical $(m, n = 2, 3)$ NTV torque (a) with E_r roots determined using flat c_p profiles, with scaled amplitude as indicated in the key. (b) Location of radial electric field roots along minor radius for each torque curve in (a).

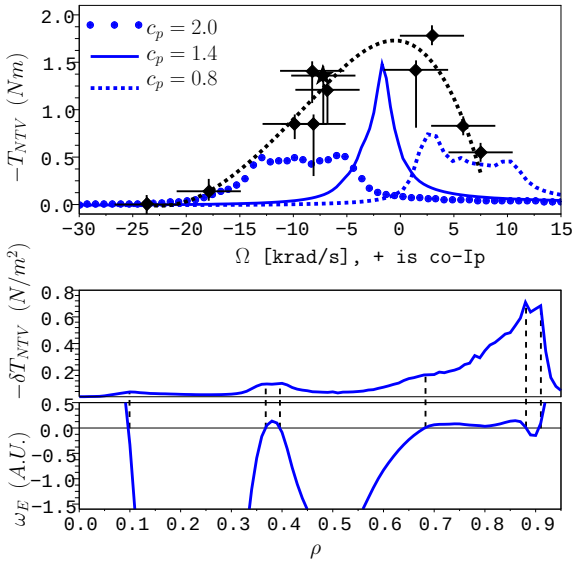

FIG. 8: (Color online) Total cylindrical $(m, n = 2, 3)$ NTV torque (a) integrated over the plasma profile as a function of Ω at $\rho = 0.67$; symbols are as in Fig. 5. Varying only the poloidal rotation value, c_p, the best fit is $c_p = 1.4$ (solid line) bracketed by two other curves with $c_p = 1.4 \pm 0.6$ respectively. Representative torque density (b) for $c_p = 1.4$, which has local maxima (and one inflection point) where $\omega_E \simeq 0$ (c) and indicated with vertical dashed lines.